Wind Uplift Strength of Trapezoidal Steel Cladding with Closely Spaced Ribs

By Dhammika Mahaarachchi[1] and Mahen Mahendran[2]

ABSTRACT

When crest-fixed thin trapezoidal steel cladding with closely spaced ribs is subjected to wind uplift/suction forces, local dimpling or pull-through failures occur prematurely at their screw connections because of the large stress concentrations in the cladding under the screw heads. Currently, the design of crest-fixed profiled steel cladding is mainly based on time consuming and expensive laboratory tests due to the lack of adequate design rules. In this research, a shell finite element model of crest-fixed trapezoidal steel cladding with closely spaced ribs was developed and validated using experimental results. The finite element model included a recently developed splitting criterion and other advanced features including geometric imperfections, buckling effects, contact modelling and hyperelastic behaviour of neoprene washers, and was used in a detailed parametric study to develop suitable design formulae for local failures. This paper presents the details of the finite element analyses, large scale experiments and their results including the new wind uplift design strength formulae for trapezoidal steel cladding with closely spaced ribs. The new design formulae can be used to achieve both safe and optimized solutions.

Keywords: Wind uplift strength, Trapezoidal cladding with closely spaced ribs, Local dimpling and pull-through failures, Finite element analyses, Experiments, Roof and wall cladding

[1] PhD Research Scholar

[2] Professor of Structural Engineering, Faculty of Built Environment and Engineering, Queensland University of Technology, Brisbane, Australia

1 INTRODUCTION

Thin high strength trapezoidal steel cladding with closely spaced ribs is commonly used as roof and wall cladding in houses, low-rise commercial and industrial buildings due to their greater spanning capacity and competitive cost. This steel cladding is often intermittently fastened at alternate crests with screw fasteners to timber or steel purlins/battens. Hence they suffer from large cross-sectional distortion when subjected to wind uplift/suction loading during high wind events such as storms and cyclones (Mahendran, 1994a). In the case of trapezoidal steel cladding with closely spaced ribs shown in Figure 1, large cross-sectional distortion then leads to local dimpling or pull-through failures which occur prematurely at their screw connections because of the large stress concentrations in the sheeting under the screw heads (see Figure 2). As seen in Figure 2(a) localised dimpling under the screw head is permanent and such local dimpling failures can cause a severe reduction to the fatigue life of steel cladding. Once the crests are dimpled, severe fatigue cracks develop around the fastener holes leading to pull-through failures under fluctuating wind forces that occur during high wind events (Mahendran, 1990a,b 1994a,b, Xu, 1995). As seen in Figure 2(b), some trapezoidal steel cladding with closely spaced ribs also suffer from pull-through failures instead of local dimpling depending on the profile geometry. These pull-through failures are initiated by transverse splitting/fracture at the screw fastener holes. During high wind events, both these local failure modes lead to loss of cladding followed by severe damage to buildings and their contents. Therefore the local dimpling or pull-through failure load is an important parameter governing the wind uplift/suction strength of crest-fixed trapezoidal steel cladding. However, in Australia there are no adequate design

guidelines for the design of steel roof and wall cladding under the governing load case of wind uplift. European and American recommendations (Eurocode, 1992, AISI, 1996) for steel cladding cannot be used as compared with Australian steel cladding, they are made of thicker (> 0.6 mm), deeper and softer steel cladding (yield stress < 450 MPa) fastened at valleys while Australian steel claddings are commonly made of thin, high strength steel G550 (0.42 mm, minimum yield stress > 550 MPa), and are crest-fixed. Although the American design formulae for screwed connections in tension are now included in the Australian cold-formed steel structures code (SA, 2005), the design of Australian profiled steel cladding to withstand design wind events is mainly based on time consuming and expensive laboratory tests. The current design formulae were found to over-predict the local dimpling/pull-through strength of crest-fixed steel cladding systems (Mahaarachchi and Mahendran, 2008).

When the less ductile G550 steel trapezoidal claddings with closely spaced ribs are subjected to local pull-through failures associated with transverse splitting/fracture at the fastener holes, numerical studies have not been able to determine the pull-through failure loads accurately (Mahendran, 1994a, Xu and Teng, 1994, Mahendran and Tang, 1999). However, an appropriate splitting/fracture criterion has been developed recently using a series of large scale experiments of crest-fixed steel cladding (Mahaarachchi and Mahendran, 2008). A shell finite element model of crest-fixed trapezoidal steel cladding with closely spaced ribs was then developed that included the new splitting criterion and other advanced features including geometric imperfections, buckling effects, contact modelling and hyperelastic behaviour of neoprene washers. Numerical results compared well with the corresponding results from large scale experiments. The finite element model was then used to study the

effects of important geometry parameters on the behaviour and strength of trapezoidal steel cladding. The results were also used to develop strength formulae that can be used to optimise the profile geometry and simplify the current design methods of trapezoidal steel cladding with closely spaced ribs. A similar investigation was also undertaken for trapezoidal steel cladding with wide pans (ie. ribs are separated by a wide pan) and the details of this investigation and the results are available in Mahaarachchi and Mahendran (2004).

In this research a static uniform wind uplift pressure was used in both numerical and experimental studies although the wind uplift pressures on roof cladding fluctuate randomly in space and time during high wind events. Details of wind loading cycles in high wind events and their fatigue effects on roof cladding are available in Kumar (2000), Kumar and Stathopoulos (1998), Jancauskas et al. (1994) and Mahendran (1995). In the experimental studies it is difficult to simulate higher pressures along the edges of cladding while simulating the variation of wind pressure loading with time makes the numerical studies complicated. Hence a static uniform wind uplift pressure was used in both numerical and experimental studies. This simplified approach allows the determination of static wind uplift strength of steel cladding systems. Since the static wind uplift strength correlates well with their fatigue uplift strength under cyclic wind uplift pressures (Mahendran, 1990b), appropriate cyclic wind uplift tests can then be undertaken to determine a suitable reduction factor to allow for the fatigue effects caused by fluctuating wind forces. By combining the results from static and cyclic wind uplift studies, steel cladding systems can be safely designed to withstand fluctuating wind uplift pressure loading. This research concentrates on the behaviour and strength of steel cladding under static uniform wind uplift pressure loading.

This paper presents the details of the investigation into the structural behaviour of trapezoidal steel cladding with closely spaced ribs under static wind uplift pressure loading. It includes finite element analyses, large scale experiments, their results and design strength formulae.

2. EXPERIMENTAL STUDY

In the analysis and testing of multi-span steel cladding assemblies, the use of a two-span steel cladding assembly with simply supported ends has been considered adequate to model the critical regions of a multi-span cladding system under a uniform wind uplift pressure (Mahendran 1990a, 1994a). Therefore in this experimental study, a two-span cladding assembly with simply supported ends was tested under a uniform wind uplift pressure loading in a rectangular air box of dimensions 1800 mm x 4200 mm x 300 mm (see Figures 3 (a) and (b)). The test cladding assembly was set-up up side down inside the air-box, which was then sealed with 4.5 μm polythene sheets. The uniform wind uplift pressure was simulated by extracting the air from the air box using a vacuum pump. Most of the test cladding assemblies were 800 mm wide (one sheet wide) × 2400 mm long (each span 900 to 1100 mm). The gaps on both sides of the cladding assembly were filled with polystyrene foam.

AS 4040.2 (SA, 1992) recommends cladding tests with two sheets in order to model the longitudinal lap between the sheets in the prototype cladding assembly. However, laboratory experiments showed that the inclined plate along the unsupported edge of the cladding buckled locally at a very low upward wind pressure. This led to larger

deformations in the pan, next to the unsupported edge. Therefore the pull-through failure of steel cladding always occurred at the second screw fastener from the unsupported longitudinal edge. This failure then led to larger loads in the adjacent fasteners, and very rapidly, led to the removal of steel sheeting. This means that there is no lateral continuity in the cladding assembly and the longitudinal lap between the two sheets has only a marginal effect. The results from single and two-sheet cladding assemblies were approximately the same. Hence only a single sheet cladding assembly was used in this investigation (see Figure 3(a)).

The trapezoidal steel claddings with closely spaced ribs (Figure 1) were fastened at alternate crests as recommended by the manufacturers. The No.14-10x50 mm Type 17 self-drilling screws with neoprene washers were used to secure the cladding to the timber supports. All the screws were centred at the crests, set perpendicular to the plane of the sheet and tightened until the neoprene washers were just prevented from rotating to avoid over-tightened or loose screws.

The load per fastener at the central support is the most important parameter controlling the local pull-through or dimpling failures (Mahendran, 1994a,b). Past research (Mahendran, 1990a, 1994a, Xu and Teng, 1994) has used approximate methods to calculate the fastener load by dividing the total central support reaction by equivalent number of fasteners at the central support due to the difficulty in measuring the exact fastener load. However, the use of the so-called average fastener load is inaccurate since it does not consider the stiffness variation across the steel cladding that has two unsupported longitudinal edges. Therefore two 5 kN load cells were used to measure the actual fastener loads in two of the central support fasteners. For this purpose the crests of cladding and the central support purlin were predrilled for the insertion of

specially made screws. These special screws had the same No.14-10 screw heads, but had a longer shaft (300 mm). The 5 kN load cells were inserted within the longer shaft and tightened with end plates. In addition to the measurement of individual fastener loads at the central support, the reaction forces at the ends of central and end support purlins were also measured using four 30 kN load cells. The latter measurements enabled the determination of the average load per fastener at the central support.

It was observed that the uplift loading caused both longitudinal and transverse bending actions in the sheeting and severe cross-sectional distortions of the profile since it was fixed at alternate crests. This distortion led to large stress concentrations around the fastener holes and premature local dimpling failures occurred at the second crest from the free longitudinal edge of the cladding assembly (see Figure 2(a)). When this screwed crest dimpled the load was transferred to other crests, which led to rapid failure of the cladding. This meant variation of fastener load across the cross-section during the local dimpling process. This behaviour was accurately captured in the experiments by using individual load cells at the central support.

In order to accurately determine the strains in the cladding in the vicinity of central support fasteners, eight strain gauge rosettes (2 mm gauge length) were used in each test. Combined membrane and bending actions in both longitudinal and transverse directions were observed in the region around the fastener holes. The membrane strains appeared to be more dominant than the bending strains in the longitudinal direction. In the case of trapezoidal claddings with wide pans, this led to transverse splitting caused pull-through failures (Mahaarachchi and Mahendran, 2008). However, in all the three large scale experiments on trapezoidal cladding with closely spaced ribs, pull-through failures were not observed, instead the screwed crests dimpled and

underwent large plastic deformations. Past research (Mahendran and Tang, 1999) has shown that the occurrence of local pull-through failures associated with transverse splitting depends on the profile geometry and hence this failure mode can be expected for this cladding with a different geometry. With further loading, considerable reserve strength was observed beyond this local dimpling failure in the two-span cladding tests. This was mainly due to an overall membrane action in the cladding system. Mahendran (1990a) has shown that any reserve static strength beyond the local dimpling failure load does not eliminate the rapid fatigue cracking in the dimpled region and premature pull-through failures during fluctuating wind forces. Therefore the reserve strength beyond the local dimpling load was ignored in this analysis.

Following extensive investigation of measured strains around the fastener holes for a range of trapezoidal steel claddings with different geometry, Mahaarachchi and Mahendran (2008) developed the following strain criterion for the fracture/splitting observed in crest-fixed profiled steel claddings. Transverse splitting/fracture occurs when

- The longitudinal membrane tensile strain is greater than 60% of the total tensile strain at the edge of the fastener holes and
- The total tensile strain is equal to the relevant measured fracture strain from tensile coupon tests of steel.

Deciding on a relevant fracture strain has been a complex process due to the significant variations in the measured fracture strain in 0.42 mm G550 steel tensile coupon tests and the difficulties in relating fractures in tensile coupon test and bending test of cladding. Therefore, the minimum measured failure strain in tensile coupon

tests based on 5 or 15 mm gauge length, i.e., 2%, was used for 0.42 mm G550 steel. Further details of the experimental investigation and the results can be found in Mahaarachchi and Mahendran (2008).

3. FINITE ELEMENT ANALYSES

3.1 Details of finite element model

The same single sheet wide two-span trapezoidal cladding assemblies with closely spaced ribs as used in the experimental study were analysed using a finite element program ABAQUS to study their behaviour under a uniform wind uplift pressure loading. ABAQUS version 5.8 (HKS, 1998) was used for all the finite element analyses (FEA) described in this paper. Two different finite element models were considered to simulate the structural behaviour of trapezoidal steel cladding systems including steel sheeting and screw fasteners. They are:

(i) Half width experimental FEA model used for comparison with large scale experimental results (Mahaarachchi and Mahendran, 2008). This model comprised only one span and half the width of sheeting.

(ii) One rib FEA model as used by other researchers (Mahendran 1994a, Tang and Mahendran 1999, Xu and Teng 1994). This model comprised only one span and a width equal to the pitch of the trapezoidal cladding.

These models were used based on relevant symmetry conditions that are present along the central support and longitudinal edges as described later in Section 3.1.4.

3.1.1 Elements

Shell elements (S4R5) were used to model the steel cladding from the ABAQUS element library (HKS, 1998) to take into account the large deformations of thin steel claddings and the localised yielding and large deformations of sheeting around the fastener holes. The S4R5 elements are thin, shear flexible, isoparametric quadrilateral shell with four nodes and five degrees of freedom per node, utilizing reduced integration and bi-linear interpolation schemes. They can be used to model both the in-plane membrane and bending actions in the sheeting, large cross-sectional distortions, both geometric and material nonlinearities, spread of plasticity effects and local buckling effects. Therefore the experimental behaviour of steel claddings could be simulated accurately.

Three dimensional eight noded continuum elements C3D8 were used to model the screw head. Experimental investigations showed that the hyperelastic behaviour of neoprene washers located between the screw head and sheeting (Figure 1) is elastic but highly nonlinear. The deformation of hyperelastic material remains elastic up to large strain values. ABAQUS hybrid elements, C3D8H three dimensional eight noded continuum elements, were therefore selected to model accurately the hyperelastic behaviour of neoprene washers. In modelling the hyperelastic behaviour, it is assumed that the material behaviour is elastic, isotropic and incompressible, and the simulation will include nonlinear geometric effects.

3.1.2 Finite element mesh

Selection of mesh size and layout is critical in finite element modelling. Convergence studies were used to choose adequate numbers of elements both across the ribs and along the ribs in order to obtain sufficient accuracy of results without excessive use of computer time.

As shown in Figure 4 (a), a finer mesh was used around the fastener holes due to the presence of rapidly varying, high local stresses and deformations in the steel sheeting. Detailed convergence studies indicated that an element size of 1 to 2 mm produced accurate results for local yielding, dimpling and pull-through failures around the fastener holes. In order to model the possible local buckling deformations in the inclined plate along the free longitudinal edge of sheeting, a finer finite element mesh had to be used. For this purpose four elements (7 to 12 mm) were used for the inclined plate while six elements (5 to 8 mm) were used for the pan. In order to maintain an optimal aspect ratio, it was necessary to have an element length of 12 mm to 14 mm in the longitudinal direction along the span. But closer to the fastener hole, it was again kept at 1 to 2 mm. There were 10 elements across the crest width of the cladding at every screwed crest and six elements were generated in the unscrewed crests. For all the models, the aspect ratio was close to one for all the elements, except for those on the crest of the claddings, away from the fastener hole and strip, in line with the support. These elements had different aspect ratios with a maximum of three and half. To model the spread of plasticity, the recommended value of five integration points through the thickness of the element was considered to be sufficient. The geometry and finite element mesh for the typical half width experimental and one rib models of trapezoidal claddings with closely spaced ribs are shown in Figures 4 (a) and (b).

3.1.3 Material properties

For both FEA models, the material was modelled as elastic perfect plastic as the 0.42 mm G550 high strength steel exhibited very little strain hardening. The material properties for the steel used were: Young's modulus = 200,000 MPa, Poisson's ratio = 0.3 and Yield (0.2% proof) stress = 690 MPa. The yield stress was based on tensile tests on specimens cut in the longitudinal direction. Tensile coupons taken in the longitudinal and transverse directions of 0.42 mm G550 steel gave different yield stresses and failure strains. Since the differences were not significant, isotropic material properties were assumed in this research. For screw heads, Young's modulus and Poisson's ratio were taken as 200,000 MPa and 0.3, respectively. For the 2 mm neoprene washer modelled as a hyperelastic material, ABAQUS was provided with experimental test data obtained from uni-axial compression test of neoprene washers (Tang and Mahendran, 1999).

3.1.4 Loads and boundary conditions

ABAQUS permits the application of pressure loads on shell elements as follower loads. A uniform surface pressure across all shell elements was considered suitable in representing the static wind uplift/suction pressure loading adequately.

Figures 4 (b) and (c) show the boundary conditions used. Due to the presence of symmetry conditions, the nodes on the planes of symmetry were constrained from translation perpendicular to the plane of symmetry and rotation about the in-plane

axis. Symmetry plane conditions were assumed along the central support for both one rib and half width experimental models. For the one rib model, symmetry conditions were assumed for both longitudinal edges whereas one of the longitudinal edges of the half width experimental FEA model was considered free as in the experiments. The transverse sheeting edge near the end support was assumed to be free to move as only the screw head holds down the cladding assemblies. Top layer of nodes of the screw heads were constrained against all three translations.

Constraint conditions between steel sheeting, neoprene washer and screw head were modelled adequately by including the presence of the 2 mm neoprene washer between the screw head and steel sheeting. For this purpose, master slave contact pair option was used. The neoprene washer is only used to prevent water leakage through the fastener hole. However, it can affect the localised deformations and stresses in the thin steel sheeting around the fastener hole. Therefore the contact surfaces between steel sheet, neoprene washer and screw head were modelled as tied contact. The tied contact bonds the contact surfaces to each other, thus eliminating severe discontinuities. It is computationally more efficient. When using the contact pair option the slave and master surfaces were correctly chosen to achieve the best possible contact simulation. In this simulation, the washers were selected as slave surfaces with finer mesh since they are softer than others.

Experiments showed that the nodes at the edge of fastener holes were moving away from the screw shaft. Therefore, both X and Y translations of these nodes should be assumed free. However, the effect of screw shaft on the in-plane movement of sheeting must be considered. Although the screw shaft may not have any effect on the

local dimpling or pull-through failure load, it prevents the in-plane movement of sheeting that can arise due to the lateral component of the applied pressure loading. The in-plane movement is prevented at the longitudinal tangential point of the left side edge of the screw through the bearing action between sheeting and the screw shaft. Therefore, this node at each fastener hole (see Figure 4 (a)) was restrained against in-plane movement, to simulate the overall effects of the screw shafts. The top layer of nodes of the screw heads was constrained against all three translations. The screw shaft was not modelled since the very small elongation of the screw shaft (0.01 mm) that can occur under the fastener tension load of 2000 N will have a negligible effect on the sheeting behaviour. The bearing action between the sheeting and the screw shaft was simulated adequately by restraining one node for each fastener hole as described above.

This research did not consider the effect of over-tightening of screw fasteners as the manufacturer's recommendation (LBI, 1997) was to insert the screw fasteners until the neoprene washer begins to compress under the screw head, ie. no over-tightening.

3.1.5 Splitting/fracture criterion

In these analyses it is necessary to compare the strains with the fracture criterion as some trapezoidal claddings with closely spaced ribs locally dimpled under the screw heads while others suffered from a local pull-though failure associated with transverse splitting. Therefore the splitting/fracture criterion developed from experiments was modelled using ABAQUS USER SUBROUTINES option. The criterion was included

using the URDFIL Fortran user subroutines. The subroutine URDFIL is called up once at the end of each increment, when new information is written to the result file.

The extraction of strain at section points in the top, bottom, and centre surfaces from the ABAQUS results file allows the calculation of the membrane and total strains and the percentage of membrane strain to total strain for every element. The values of these parameters are then compared with the splitting/fracture criterion. When the criterion is met in any element, it terminates the analysis and sends a message to the message file giving the reason for the termination of the analysis.

3.1.6 Initial imperfections

In the nonlinear analysis of steel members subject to local buckling it was necessary to include local imperfections. For the half width experimental model, it was necessary to include the local imperfections in order to allow for possible local buckling along the free longitudinal edges of sheeting. Initial geometric imperfections were modelled by providing initial out-of-plane deflections to the model. The first elastic buckling mode shape for wind uplift was used to create the geometric imperfections (see Figure 5). The maximum amplitude of the buckled shape determined the level of imperfection. Since there are no measured data available for the magnitude of imperfections of steel claddings, a local buckling imperfection of w/167 was chosen as recommended by Schafer and Pekoz (1998) for cold-formed steel members subject to local buckling. Nonlinear analyses showed the insignificant effect of imperfections on the ultimate failure load. However, the deformation pattern allowed the post-buckling deformations to proceed correctly and hence convergence

was achieved faster compared with analyses having a zero imperfection. The one rib model was not subjected to local buckling effects due to the absence of free longitudinal edges, and therefore geometric imperfections were not used in the nonlinear analysis of one rib models.

Since the nonlinear analyses of trapezoidal claddings with wide pans showed that residual stresses have only a small effect (less than 0.08%) on the ultimate failure load (Mahaarachchi and Mahendran, 2004), residual stresses were not included in this study.

3.1.6 Analysis

Both elastic buckling and nonlinear static analyses were used. Elastic buckling analyses were used to obtain the eigenvectors for the geometric imperfections. Nonlinear static analysis including the effects of large deformation and material yielding was adopted to investigate the ultimate strength behaviour of steel claddings. The RIKS method in ABAQUS, generally used to predict unstable geometrically nonlinear collapse of structures, was also included in the analysis. In using the RIKS method in this study, the solution of nonlinear equations was achieved by Newton-Raphson method in conjunction with a variable arc-length constraint to trace the instability problems associated with local dimpling of crests in the sheeting.

3.2 Model validation

All the necessary convergence studies and sensitivity analyses were carried out before the detailed analyses. In order to validate the accuracy of the chosen finite element model in predicting the local dimpling or pull-through failure loads, the FEA results for 0.42 mm G550 steel trapezoidal claddings with closely spaced ribs were compared with the corresponding experimental results. The FEA results confirmed that significant cross-sectional distortions occurred in the cladding with the unscrewed crests deflecting upward quite significantly (see Figures 6 and 7(c)). Therefore this led to a premature localised failure of the crests. At first the crests slightly dimpled (see Figure 7(a)), which was followed by the longitudinal membrane action of the region. The region around the fastener hole was yielding at this stage. All of these observations are very similar to those observed in the two-span cladding experiments (see Figure 7(b)).

Following the verification of local and overall deformation shapes (Figures 6 and 7), comparison of the load-deflection curves were made with the two-span experimental results for 0.42 mm trapezoidal cladding of 1100 mm span. Figures 8 (a) and (b) show good agreement between the load-deflection curves obtained from the FEA and two-span cladding experiments, which further validates the accuracy of the advanced FEA model used in this study. In these figures, upward deflections of unscrewed crests at mid-span and central support are used. For one rib FEA models, the average experimental load per fastener was used in the comparison whereas for the half width experimental FEA model, the actual fastener load was used. It is seen that the results from the half width model are in close agreement with the experimental results in the case of actual measured fastener load. In contrast, the results from the one-rib finite element model agreed well only when the average fastener load was used. The

measured experimental fastener failure load of 1040 N agreed very closely with the failure load of 1067 N predicted by the half width experimental model for the corresponding fastener location (2^{nd} from the free longitudinal edge). This is also confirmed by the comparisons presented in Table 1, using the results from half width finite element model and the three large scale experimental results.

It is important to note that FEA predicted an instability problem when the local dimpling load was reached. There was a sudden drop in the load with large deformations, but the load increased again. The same observation was made in the experiments and this further validates the finite element model's ability to simulate the true behaviour of steel claddings including both the local instability and further strengthening stages (see Figure 8).

In the past research (Mahendran, 1994a, Tang and Mahendran 1999), it was not possible to model the splitting/fracture caused pull-through failure observed in some trapezoidal steel claddings made of high strength steels. Even though the available test results on trapezoidal claddings with closely spaced ribs showed that only localised dimpling failures occurred, this cannot be true for other profile geometries. Therefore, the fracture/splitting criterion developed in the experimental investigation was used in this study to investigate the splitting/fracture behaviour of this cladding. As observed in the experiments, the FEA did not predict fracture for the tested trapezoidal claddings considered here (see Figure 8 and Table 1), which indicates that the splitting/fracture criterion enables accurate prediction of the behaviour of crest-fixed steel claddings. The same criterion has also been used successfully to predict the

pull-through failures associated with fractures for other steel cladding profiles (Mahaarachchi and Mahendran, 2004).

3.3 Discussion of Results

Past research (Mahendran, 1994a, Xu and Teng, 1994) has always considered the use of one rib finite element model to be adequate because of the symmetric conditions of geometry and loading present in a two-span cladding system. This simple model is computationally efficient, but assumes continuos sheeting in the transverse direction and ignores the presence of longitudinal laps between sheets. Experimental studies have revealed the absence of such lateral continuity. The results from single and two-sheet cladding assemblies were approximately the same (Mahaarachchi and Mahendran 2008). In the half width finite element model, the symmetry conditions were applied only along the symmetry plane and hence it simulated the real situation more closely.

Experiments showed that the local dimpling failure is governed by the magnitude of the fastener load. The one rib FEA model predicted a failure load of 1140 N for the cladding of 1100 mm span, which agrees well only with the average experimental load per fastener of 1143 N (see Table 2). However, the experiments revealed that the measured individual load per fastener is less than the average load per fastener because the average load per fastener calculations do not consider the stiffness variation across the sheet due to lateral discontinuity between sheets.

This phenomenon was clearly seen in the half width experimental FEA model. The half width model showed that the fastener load was not uniform among the fasteners.

Second fastener from the free edge always had the highest load near the failure. This is very similar to that observed in the two span cladding tests where most of the failures occurred at the same location. The half width finite element model predicted a failure load of 1067 N, which agrees very well with the measured individual fastener load of 1040 N. In contrast, the one rib finite element model over-predicted the failure load (1140 N). All of these observations indicate that the half width model and not the one rib model must be used in simulating the true behaviour of two-span profiled steel claddings. Similar observations were also made in the investigation on trapezoidal claddings with wide pans (Mahaarachchi and Mahendran, 2004). Therefore in the detailed parametric studies of trapezoidal claddings with closely spaced ribs, half width experimental FEA model was used.

4 PARAMETRIC STUDIES

The half width experimental FEA model discussed in the previous section was used to determine the local dimpling and pull-through failure loads of a range of trapezoidal steel claddings with closely spaced ribs. The following parameters including all important dimensions of the trapezoidal claddings were varied in this study (see Figure 9): Base metal thickness of steel t from 0.42 mm to 0.8 mm (0.42, 0.6, 0.8); steel yield stress f_y of 250 and 690 MPa (as appropriate for G250 and G550 grade steels); Young's modulus E from 150 to 250 GPa; diameter of screw head or washer d from 10 to 22 mm; crest width w_c from 17.5 to 35 mm; crest height h_c from 17 to 50 mm; pitch p from 70 to 130 mm; trough width w_t from 55 to 80 mm; and span L from 600 to 1400 mm. In each case, all the possible variations were considered, which lead to a total of 228 finite element analyses. In some cases, variations were beyond the actual

values, for example, Young's modulus E, but they were considered for the sake of gaining more data from the parametric study.

In this parametric study, the 2% minimum measured fracture strain value obtained from the tensile coupon tests was used as the total strain in the fracture criterion for 0.42 mm G550 steel. This will lead to conservative design formulae. For 0.6 and 0.8 mm G550 steels, fracture strain values of 6 and 7% were used as specified by the manufacturers as the minimum fracture strain (BHP, 2002). For lower grade ductile steel (G250), the measured fracture strain from the tensile coupon test of 25% was used as the fracture strain was high and its variation was small.

With the inclusion of an appropriate fracture criterion, the finite element analyses were able to determine both the local dimpling and pull-through failure loads. If there was a fracture based on the used criterion, the FEA indicated the occurrence of pull-through failure. As indicated earlier in this paper, both failure loads are to be considered the ultimate loads in the design of steel claddings to withstand high wind events. Therefore in the parametric study, no distinction was made between the two local failure loads and a common term, fastener failure load, $F_{ov,}$ was used.

The behaviour of thin, high strength crest-fixed steel claddings subjected to wind uplift loading is complex and very much dependent on a range of parameters including the profile geometry, steel thickness and yield stress. Simple relationships based on theoretical models or simple curve fitting methods could not be derived between the failure load and the many parameters considered in this investigation. Therefore, the fastener failure load interactions with geometrical and other parameters were first

analysed using Buckingham's Pi theorem. Buckingham's Pi theorem allows rearranging n variables in a given system into n-j dimensionless parameters where j is the fundamental dimension of the n variables. It reduces the number of variables in a given problem for a subsequent analysis, but does not lead to a complete solution of a physical problem. Therefore Buckingham's Pi theorem was first used to derive the dimensionless quantities and then FEA results were used to appropriately combine them.

As the fastener load at failure F_{ov} depends on the cladding profile geometry, yield stress, Young's modulus, thickness, and span, the following functional relationship is deduced from the above variables.

$$\phi\ (F_{ov,}\ f_{y,}\ E,\ h_{c,}\ p,\ d,\ w_{c,}\ w_{t,}\ L,\ t) = 0$$

Choosing the $f_{y,}$ d and t as the repeating variables following dimensionless quantities can be derived.

$$\Pi_1 = \frac{F_{ov}}{f_y dt} \quad \Pi_2 = \frac{Et}{f_y d} \quad \Pi_3 = \frac{h_c d}{t^2} \quad \Pi_4 = \frac{pd}{t^2} \quad \Pi_5 = \frac{w_c d}{t^2} \quad \Pi_6 = \frac{w_t d}{t^2} \quad \Pi_7 = \frac{Ld}{t^2} \qquad (1)$$

From the above dimensionless groups the following relationship can be written. Fastener failure load F_{ov} is obtained as

$$F_{ov} = f_y dt \quad f\left(\frac{Et}{f_y d}, \frac{h_c d}{t^2}, \frac{pd}{t^2}, \frac{w_c d}{t^2}, \frac{w_t d}{t^2}, \frac{Ld}{t^2}\right) \qquad (2)$$

There is little correlation among these derived Π parameters as the behaviour of crest-fixed trapezoidal steel cladding is complicated. The finite element analysis results have shown that the above Π parameters have a combination of linear and nonlinear relationships. Therefore, attempts were made to combine the above dimensionless quantities with nonlinear interactions considering the possible meaningful interactions of the geometric parameters. It is clear that the fastener load at failure depends on the geometry of the claddings. The approach adopted here assumed that there should be a closer relationship between the trough width (w_t) and the crest width (w_c) in defining the shape. Similarly, there is a need to use the ratio of crest height (h_c) to pitch (p) to fully define the cladding profile geometry. When the crest height is increased it is obvious that the pitch will also be increased to make the profile more economical. Therefore, the fastener failure load is considered the function of the above ratios. Rearranging these parameters leads to the following.

$$\Pi_1 = \alpha\left(\mu + \phi\Pi^{\beta}{}_2\right)^{\delta}\left(\vartheta\frac{\Pi_3}{\Pi_4}\right)^{\varepsilon}\left(\omega\frac{\Pi_5}{\Pi_6}\right)^{\lambda}\left(\kappa + \varphi\Pi_7\right)^{\rho} \tag{3}$$

Substituting relevant parameters, this equation can be rearranged as

$$F_{ov} = \alpha\left(\mu + \phi\frac{Et}{f_y d}\right)^{\delta}\left(\vartheta\frac{h_c}{p}\right)^{\varepsilon}\left(\omega\frac{w_t}{w_c}\right)^{\lambda}\left(\kappa + \varphi\frac{t^2}{Ld}\right)^{\rho} dtf_y \tag{4}$$

Different power coefficients in the above equation are determined by considering all the parameters simultaneously. The “Solver” in Microsoft Excel, which is based on the method of least squares and linear programming, was used to obtain the best equation

that fits the FEA results. Finally, the expression for local pull-through or dimpling failure load can be written as

$$F_{ov} = 0.04\left(9-\frac{33f_y d}{Et}\right)^2\left(\frac{h_c}{p}\right)^{3/4}\left(\frac{w_t}{w_c}\right)^{1/5}\left(12+\frac{1500t^2}{Ld}\right)^{1/3} dtf_y \qquad (5)$$

The local dimpling or pull-through failure loads were predicted by this equation with a mean of 1.06 and a coefficient of variation (COV) of 0.14. The results were further analysed to obtain better correlation and uniformity across the predicted values by separating them based on the steel grade. Two equations were developed for G550 and G250 steels as shown next with a mean of 1.0 with COVs of 0.12 and 0.10, respectively.

G550 grade steel

$$F_{ov} = 0.04\left(4.7-\frac{20f_y d}{Et}\right)^2\left(\frac{h_c}{p}\right)^{3/4}\left(\frac{w_t}{w_c}\right)^{1/5}\left(12+\frac{1500t^2}{Ld}\right)^{1/3} dtf_y \qquad (6)$$

G250 grade steel

$$F_{ov} = 0.008\left(9.52-\frac{49f_y d}{Et}\right)^2\left(\frac{h_c}{p}\right)^{3/4}\left(\frac{w_t}{w_c}\right)^{1/5}\left(12+\frac{1500t^2}{Ld}\right)^{1/3} dtf_y \qquad (7)$$

In this study the yield strength of steel f_y was used instead of the ultimate tensile strength f_u because for lower grade steel localised dimpling and yielding take place around the fastener holes whereas for higher grade steels Roger and Hancock (1997) have shown that the ratio of f_u/f_y is equal to one.

5 CAPACITY REDUCTION FACTORS

The proposed design equations in the last section were derived based on limited data. Therefore the actual local dimpling or pull-through failure strength of a real connection may be considerably less than the value predicted by these equations because of the expected variations in material, fabrication and loading effects. Therefore a capacity reduction factor as used in design codes is recommended for the strength predicted by the above formulae.

The American cold-formed steel structures code (AISI, 1996) and Australian cold-formed steel structures code AS/NZS 4600 (SA, 2005) recommends a statistical model for the determination of capacity reduction factors from testing. Based on this model, the capacity reduction factor ϕ is given by the following equation.

$$\phi = 1.5\, M_m F_m P_m \; e^{-\beta_0 \sqrt{V_m^2 + V_f^2 + C_p V_p^2 + V_q^2}} \qquad (8)$$

Above equation was used to calculate the reduction factor ϕ for the three design formulae (Equations 5, 6 and 7). The capacity reduction factors determined for different grades of steel claddings are shown in Table 3 (0.61 to 0.64). Australian cold-formed steel structures code recommends a factor of 0.5 for connections. Therefore, the recommended capacity reduction factor is acceptable within the current design provisions. However, the derived strength equations can be used with a higher reduction factor of 0.6 in the design of trapezoidal claddings with closely spaced ribs considered in this investigation.

6 CONCLUSIONS

This paper has described an investigation into the structural behaviour and design of crest-fixed trapezoidal steel claddings with closely spaced ribs under wind uplift/suction forces. An advanced finite element model was developed that simulated the large deformations of thin steel sheeting associated with localised dimpling and pull-through failures at the fastener holes. It was validated using large scale experimental results and was then used in a detailed parametric study. The results from the parametric study were used to develop non-dimensional design strength formulae for the fastener failure load of trapezoidal steel claddings with closely spaced ribs. This research has also shown that the commonly used one rib finite element model was unable to simulate the true behaviour of two span steel cladding assemblies. Both experiments and finite element analyses showed the presence of non-uniform fastener load variation at critical supports and hence it is recommended that the actual critical fastener failure load is used instead of the average fastener failure load. The results from this investigation including the design strength formulae can be used to develop safe and optimum solutions for trapezoidal steel cladding with closely spaced ribs under wind uplift/suction forces.

7 REFERENCES

American Iron and Steel Institute (AISI) (1996) Specification for the Design of Cold-formed Steel Structural Members, AISI, Washington, DC, USA.

BHP (2002) Product information, http://www.bhpsteel.com.au/index.cfm, [accessed 06 January 2002]

Eurocode (1992) Design of Steel Structures, Part 1.3 – Cold-formed Thin-gauge Members and Sheeting, Commission of European Communities, Brussels, Belgium.

Hibbitt, Karlsson and Sorensen (HKS) (1998) ABAQUS User's manual, Pawtucket, RI, USA.

Jancauskas, E.D., Mahendran, M. and Walker, G.R. (1994) Computer Simulation of the Fatigue Behaviour of Roof Cladding during the Passage of a Tropical Cyclone, J. of Wind Engineering and Industrial Aerodynamics, Vol.51, pp.215-227.

Kumar, K.S. (2000) Prediction of Wind-induced Fatigue on Claddings of Low Buildings, Computers and Structures, Vol.75, No.1, pp.31-44.

Kumar, K.S. and Stathopoulos, T. (1998) Fatigue Analysis of Roof Cladding Under Simulated Wind Loading, J. of Wind Engineering and Industrial Aerodynamics, Vol.77-8, pp.171-183.

Lysaght Building Industries (LBI) (1997) LBI Reference Manual, Sydney, Australia.

Mahaarachchi, D. and Mahendran, M. (2004) Finite Element Analysis and Design of Crest-fixed Trapezoidal Steel Claddings with Wide Pans subject to Pull-through Failures, Engineering Structures, Vol. 26, Issue 11, pp.1547-1559

Mahaarachchi, D. and Mahendran, M. (2008) A Strain Criterion for Pull-through

Failures in Crest-fixed Steel Claddings, Engineering Structures, Available online, DOI information: 10.1016/j.engstruct.2008.09.013

Mahendran, M. (1990a) Static Behaviour of Corrugated Roofing under Simulated Wind Loading, Civil Eng. Trans., I.E.Aust., 32(4), pp.211-218.

Mahendran, M. (1990b) Fatigue Behaviour of Corrugated Roofing under Cyclic Wind Loading, Civil Eng. Transactions, I.E. Aust., Vol. CE32, No.4, pp.219-226.

Mahendran, M. (1994a) Behaviour and Design of Crest-fixed Profiled Steel Roof Claddings under High Wind Forces, Engineering Structures, Vol.16, No 5, pp.368-376.

Mahendran, M. (1994b) Steel Roof Claddings under Simulated Cyclonic Wind Forces, Civil Eng. Transactions of I.E.Aust., Vol.36, No.1, pp.1-10

Mahendran, M. (1995) Towards an Appropriate Fatigue Loading Sequence for Roof Claddings in Cyclone Prone Areas, Engineering Structures, Vo.17, No.7, pp.476-484.

Mahendran, M. and Tang, R.B. (1999) Pull-through Strength of High Tensile Steel Cladding Systems, Australian Journal of Structural Engineering, SE2, pp.37-49.

Roger, C.A. and Hancock, G.J. (1997) Ductility of G550 Sheet Steel in Tension, Journal of Structural Engineering, Vol.123, No.12, pp.1586 – 1594.

Schafer, B.W. and Pekoz, T. (1998) Computational modelling of cold-formed steel: characterizing geometric imperfections and residual stresses, Journal of Constructional Steel Research, Vol.47, pp.193-210.

Standards Australia (SA) (2005) AS/NZS 4600 Cold-formed Steel Structures Code, Sydney, NSW, Australia.

Tang, R.B. and Mahendran, M. (1999) Pull-over Strength of Trapezoidal Steel Claddings, Proc. of the 4th Int. Conference on Steel and Aluminium Structures, Helsinki, Finland, pp.609-616.

Xu, Y.L. and Teng, J.G. (1994) Local Plastic Failures of Light Gauge Steel Roofing Sheets, Journal of Construct. Steel Research, Vol.30, pp.125-150.

Xu, Y.L. (1995) Fatigue Performance of Screw-Fastened Light-Gauge Steel Roofing Sheets, ASCE J. of Structural Engineering, Vol.121 No.3, pp.389-398.

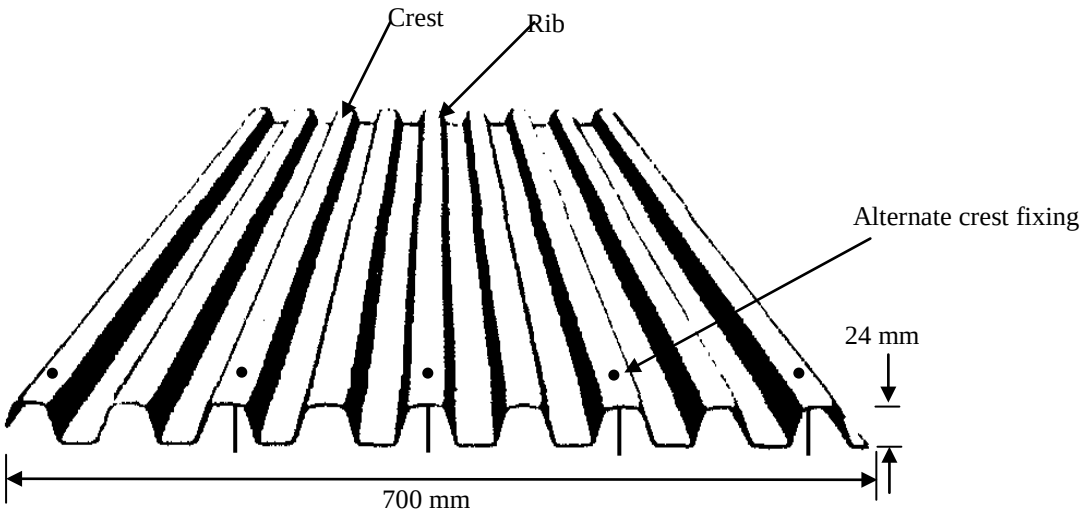

Crest width w_c = 25 mm Trough width w_t = 63 mm Pitch p = 87 mm

(a) Trapezoidal cladding profile

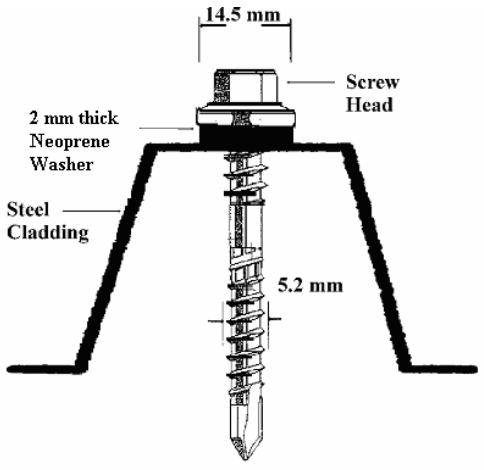

(b) Crest-fixing

Figure 1 Trapezoidal steel cladding with closely spaced ribs

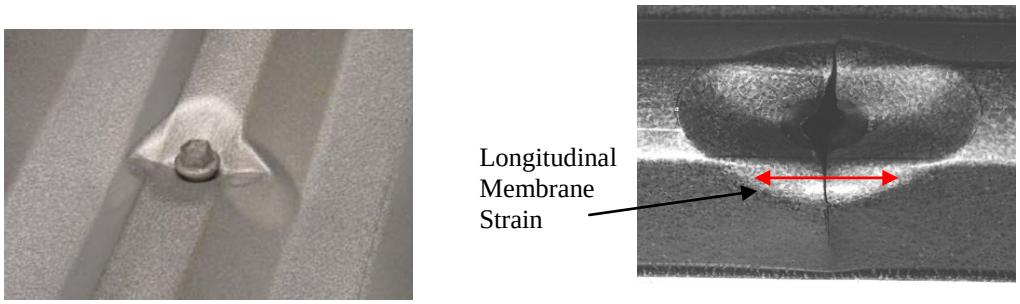

(a) Local dimpling

(b) Local pull-through failure with Transverse splitting

Figure 2 Local failures at screwed connections

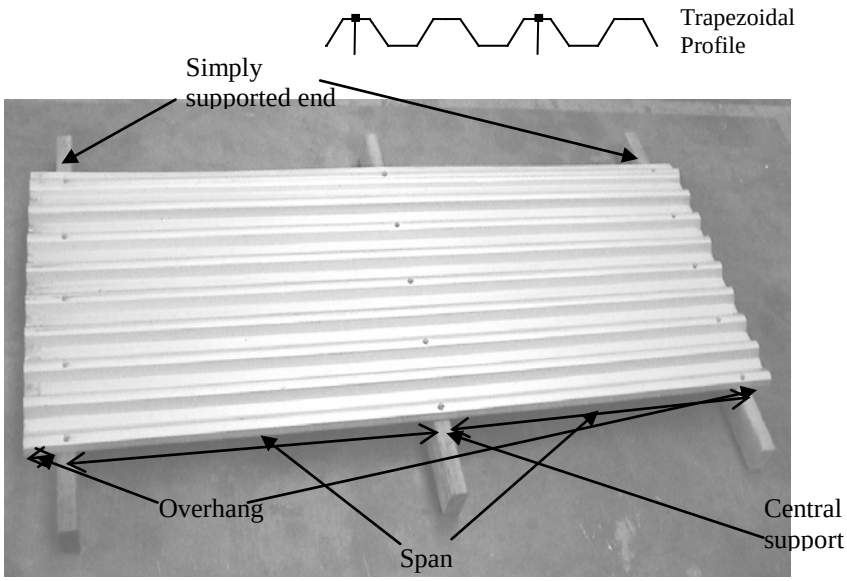

(a) Single sheet wide two-span cladding assembly

(b)

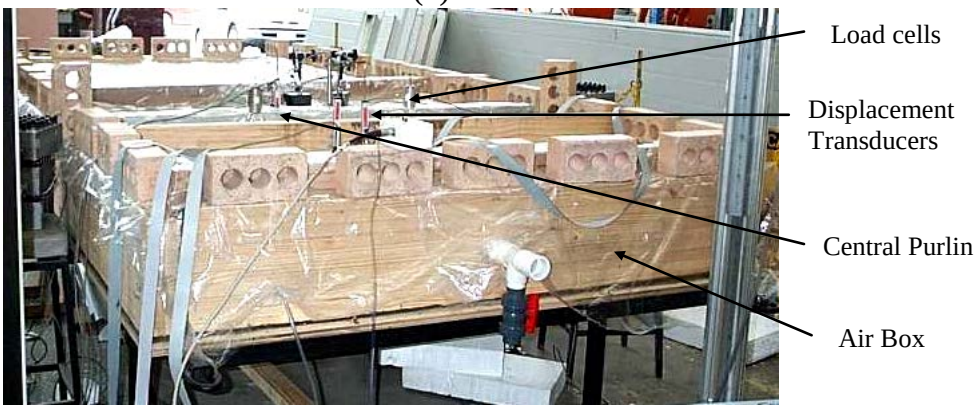

(b) Air-box

Figure 3 Experimental set-up

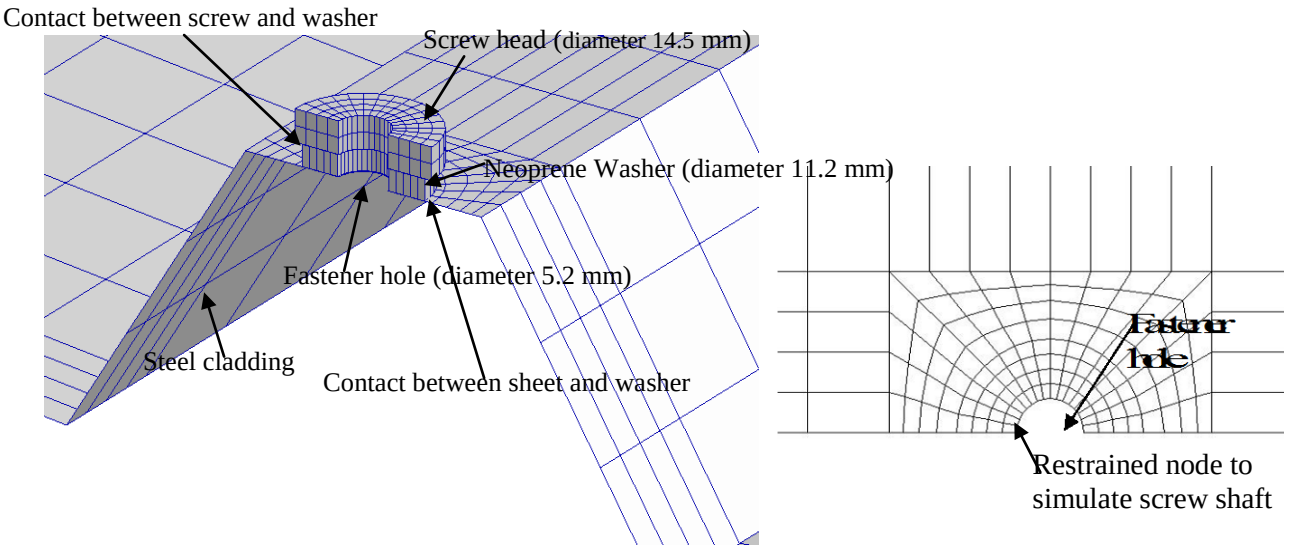

(a) Finer mesh used in the vicinity of the Fastener hole

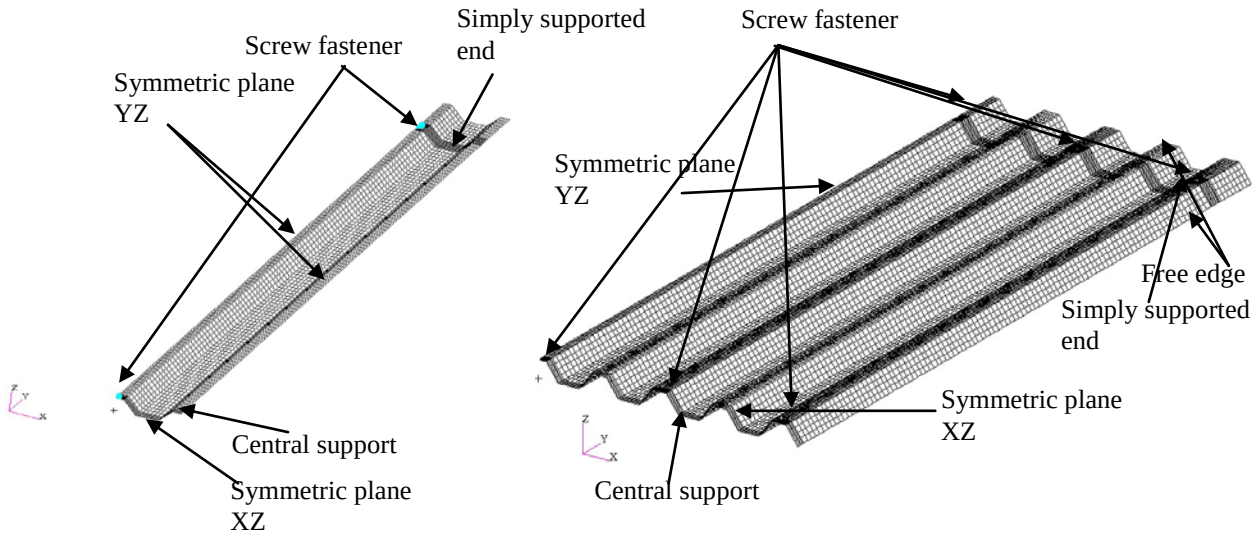

(b) One rib model

(c) Half width experimental model

Figure 4 Details of finite element modelling

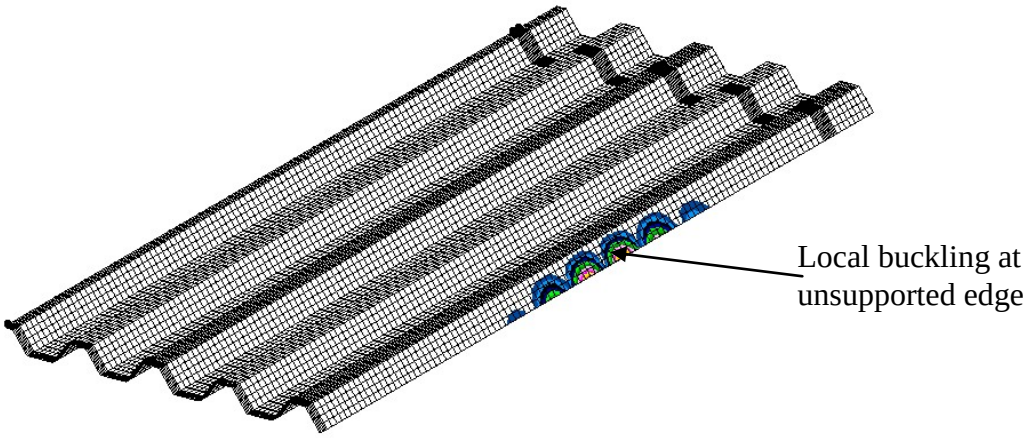

Figure 5 Inclusion of initial geometric imperfections

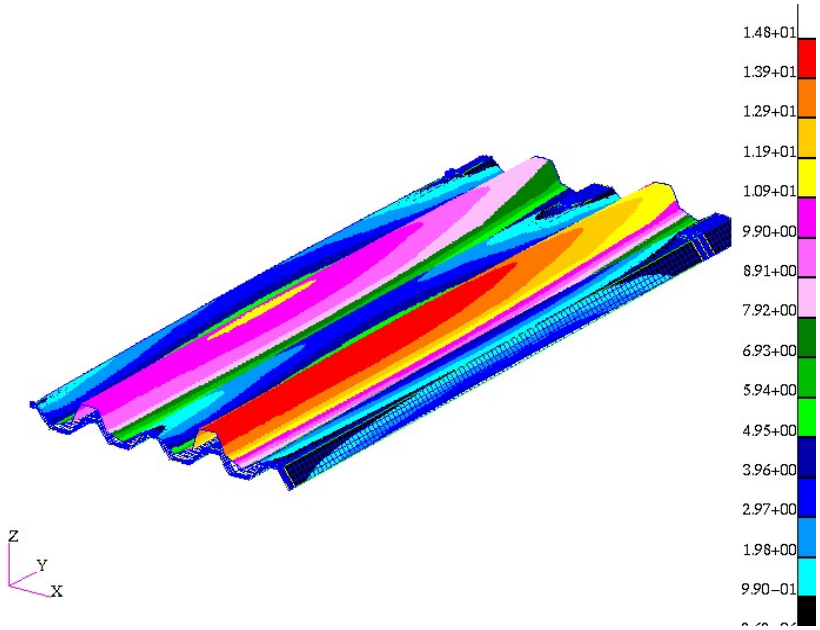

(a) Half width experimental model

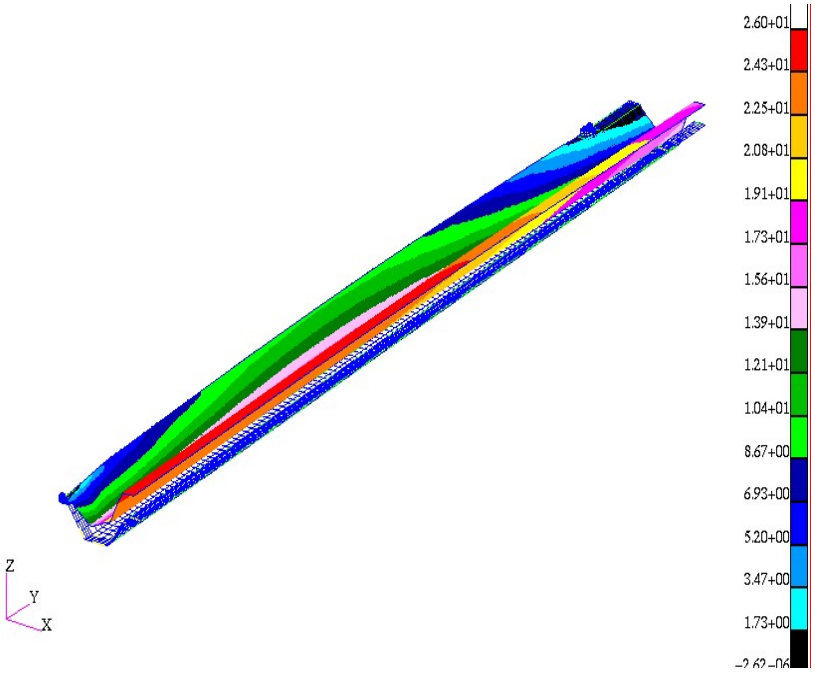

(b) One rib model

Figure 6　Overall deformations of trapezoidal cladding with closely spaced ribs

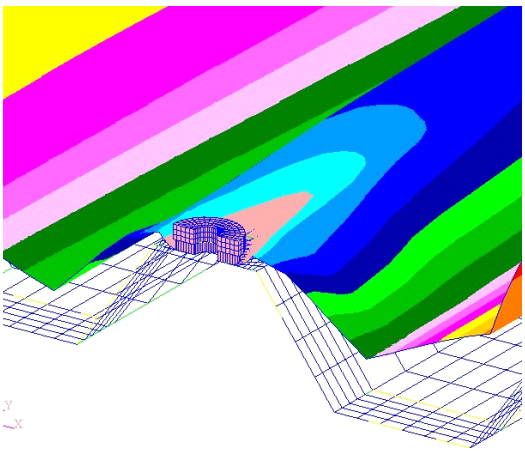

(a) FEA

(b) Experiment

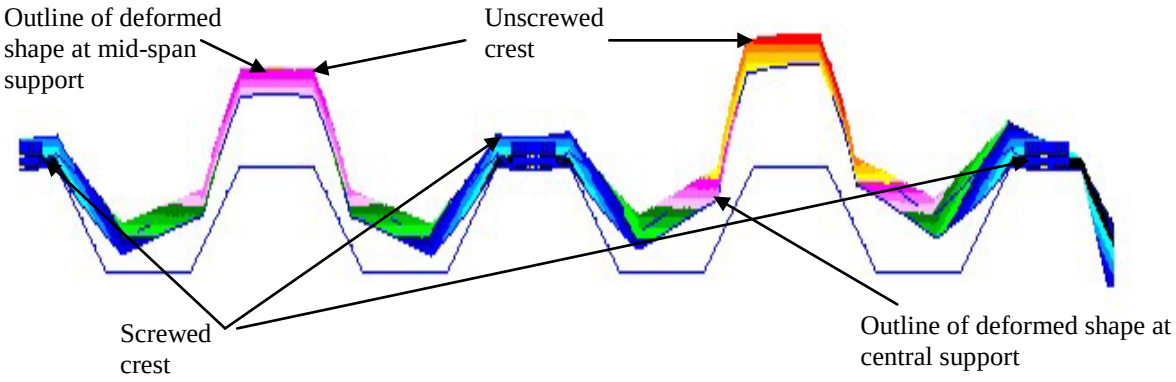

(c) Cross-sectional distortion – FEA

Figure 7 Localised deformations around the fastener hole

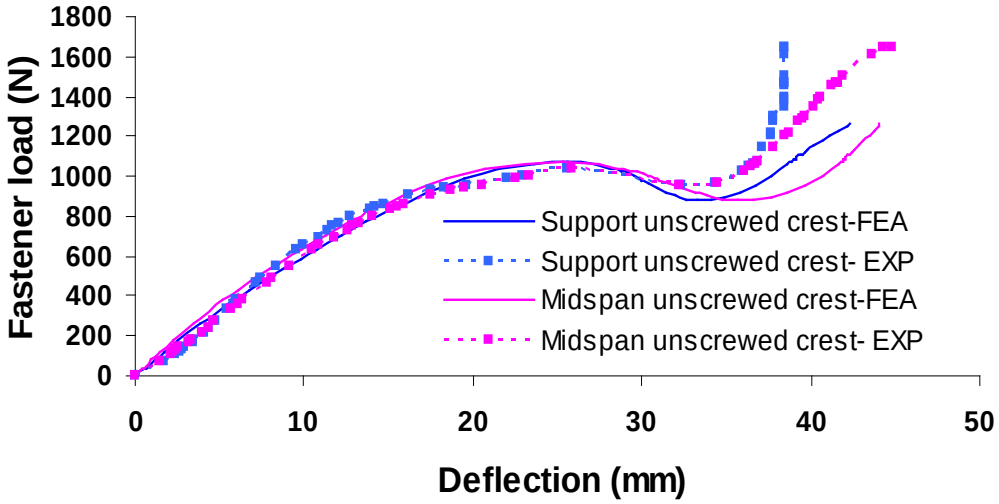

(a) Half width experimental model

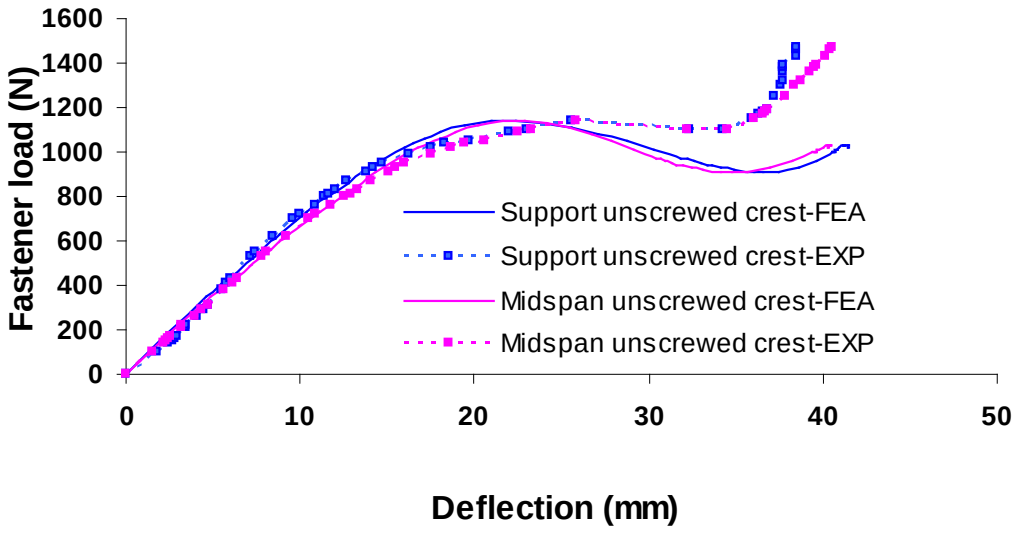

(b) One rib model

Figure 8 Comparison of load-deflection curves

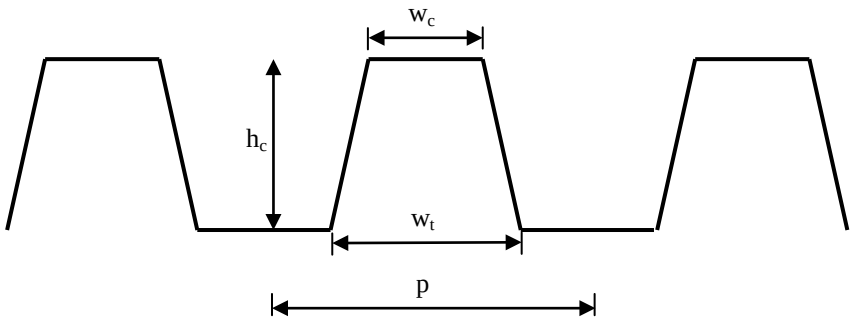

Figure 9 Geometry of trapezoidal cladding with closely spaced ribs

Table 1 Comparison of Fastener Loads at Failure for Half Width FEA Model

Span (mm)	Thickness (mm)	Fastener load at failure (N)			
		Experiment		Half Width FEA	
		Average	Measured	Without splitting criterion	With splitting criterion
900	0.42	1225	1063	1064	1064
1100	0.42	1143	1040	1067	1067
900	0.48	1543	1300	1478	1478

Table 2 Comparison of Fastener Loads at Failure for One-rib FEA Model

Span (mm)	Thickness (mm)	Fastener load at failure (N)			
		Experimental		One-rib FEA	
		Average	Measured	Without splitting criterion	With splitting criterion
900	0.42	1225	1063	1195	1195
1100	0.42	1143	1040	1140	1140
900	0.48	1543	1300	1564	1564

Table 3 Capacity Reduction Factor ϕ

Steel Grade	Thickness (mm)	Mean	COV	Number of Tests	Capacity Factor ϕ
All grades	0.42	1.06	0.14	108	0.64
	0.60			60	
	0.80			60	
G550	0.42	1.00	0.12	54	0.61
	0.60			60	
	0.80			60	
G250	0.42	1.00	0.10	54	0.63

Note: Mean and COV for each group are based on different design equations